



Evaluating the Effects of Sedimentary Cycles (Aeolian and Fluvial) on Chemical Weathering Indices in Rafsanjan Region, Southeast of Iran

Isa Esfandiarpour-Boroujeni^{1,*}, Farzaneh Bandehelahi¹, Zohreh Mosleh², Alireza Karimi³, Mohammad Hady Farpoor⁴, Morteza Fattahi⁵

¹ Soil Science Department, Faculty of Agriculture, Vali-e-Asr University of Rafsanjan, Rafsanjan, Iran

² Soil and Water Research Institute, Agricultural Research, Education and Extension Organization (AREEO), Karaj, Iran

³ Soil Science Department, Faculty of Agriculture, Ferdowsi University of Mashhad, Mashhad, Iran

⁴ Soil Science Department, Faculty of Agriculture, Shahid Bahonar University of Kerman, Kerman, Iran

⁵ Institute of Geophysics, University of Tehran, Tehran, Iran

Received: 5 November 2021, Revised: 25 December 2021, Accepted: 15 January 2022

© University of Tehran

Abstract

Chemical indices are widely used for characterizing the degree of weathering. In this study, we focused on evaluating the capability of chemical weathering indices to distinguish the sequence of aeolian-fluvial sediments in an arid region of Iran. Seven dominant geoforms were selected in Rafsanjan region, southeast of Iran, namely pediment, alluvial fan, margin of pediment and sand sheet, desert pavement, margin of fan and cultivated clay flat, active drainage, and margin of fan and uncultivated clay flat. One representative pedon was selected, described, and sampled for each geoform. The soil physicochemical properties of different horizons of each pedon were determined. We calculated various weathering indices, including weathering index of Parker (WIP), product index (PI), chemical index of alteration (CIA), silica-sesquioxide ratio (Kr), and CIA/WIP ratio (IR), and elucidated their depth distributions. The heterogeneity of the parent material within a given pedon was confirmed with field evidence, depth functions of clay-free sand fractions, and the uniformity value (UV) index. The horizon sequence with lithologic discontinuities (LDs) indicated that the studied pedons were formed by cyclic deposition of aeolian and fluvial sediments. The vertical variations of the weathering indices as well as the vertical trend of the Al_2O_3/SiO_2 ratio (as a grain size index) were entirely consistent with the presence of the LDs. The results suggested that different factors, such as grain size, sedimentation cycling, and their interactive effects, should be considered in order to accurately assess the vertical trend of chemical weathering indices.

Keywords: Geochemical composition, Grain size, Lithologic discontinuity, Sedimentation cycling

Introduction

Chemical weathering is a process in which primary minerals are transformed into new minerals. The rate of weathering and the chemical composition of sediments are generally influenced by the composition of the parent rocks (Fedo et al., 1997), chemical weathering conditions (Nesbitt and Young, 1982; Clift et al., 2008), sorting effects (Roser, 2000), and the grain size that is driven by the depositional processes (Yang et al., 2006). The ratios between mobile and immobile elements change during chemical weathering as cations have different mobilities due to differences in their ionic potentials (Roy et al., 2008). Various weathering indices, such as the chemical index of alteration (CIA; Nesbitt and Young, 1982), weathering index of Parker

* Corresponding author e-mail: esfandiarpour@vru.ac.ir

(WIP; Parker, 1970), and chemical index of weathering (CIW; Harnois, 1988), have been widely employed for quantifying and to characterizing the degree of weathering. According to Okewale (2020), it is essential to assess the chemical indices across different depths in order to characterize the degree of weathering and identify the underlying trend along the vertical profile.

Lithologic discontinuities (LDs) are defined as significant changes in the particle size distribution or mineralogy, which reflect the differences in terms of lithology and age within a soil (Soil Taxonomy, 2014). Consequently, LDs separate different sedimentary layers formed during a shift from one depositional system to another (aeolian to fluvial) or once changes take place within a single sedimentary system (differences in age or depositional energy). Lithology determines the type of the pre-existing minerals available for possible reactions, which plays an important role in the weathering process (Gaillardet et al., 1999; Chetelat et al., 2013). Additionally, several studies have confirmed that the geochemical compositions of sediments strongly correlate with the grain size distribution (Garzanti et al., 2011; Lacey et al., 2017; Hatano et al., 2019). Hatano et al. (2019) and Guo et al. (2018) demonstrated that the Al_2O_3/SiO_2 ratio is an appropriate grain size index. A study on the relationship between the chemical weathering and grain size distribution of aeolian deposits in Chinese loess plateau revealed that the impact of grain size on the chemical weathering indices is more pronounced in interglacial periods in comparison with that in glacial periods (Qin and Mu, 2011).

Our knowledge of the behavior of elements during the chemical weathering processes needs to be further improved. Several studies have explored the relationships between chemical weathering and erosion (Song et al., 2019; Derakhshan-Babaei et al., 2020), mechanical behavior of rocks (Okewale, 2020), as well as fertility and soil development (Delvaux et al., 1989). A few studies (Hatano et al., 2019; Vasu et al., 2020) have however investigated the spatial variability of weathering indices along a vertical profile, and a possible link between these indices and the heterogeneity of parent material in a quantitative manner. It is necessary to investigate whether the diverse and heterogeneous source lithology can exert significant control on the weathering indices. The main objective of the present study was to evaluate the capability of the chemical weathering indices in order to characterize the sequence of aeolian-fluvial sediments in different geomorphs in Rafsanjan region, southeast of Iran.

Materials and Methods

Study area

The study area is a part of Davaran area ($55^{\circ} 56' 43''$ to $56^{\circ} 13' 13''$ E and $30^{\circ} 27' 49''$ to $30^{\circ} 37' 20''$ N), located in 15 km east of Rafsanjan region, southeast of Iran, with an area of ~ 56 km² and a mean elevation of 1645 meters above the sea level (m.a.s.l; Fig. 1). According to a 30-year record (1989 to 2019), the mean annual temperature and precipitation of the area were 18.9 °C and 80.3 mm, respectively. The soil moisture and temperature regimes are Aridic and Thermic, respectively. The parent materials of the region include Quaternary sediments (fluvial and aeolian), originating from various rocks, like marl, shale, conglomerate, granite, sandstone, quartzite, and limestone (Geological Survey and Mineral Exploration of Iran, 2020). In general, the processes of water and wind erosion, sedimentation, along with human activities (including pistachio cultivation) have led to formation of various geomorphs in the studied area.

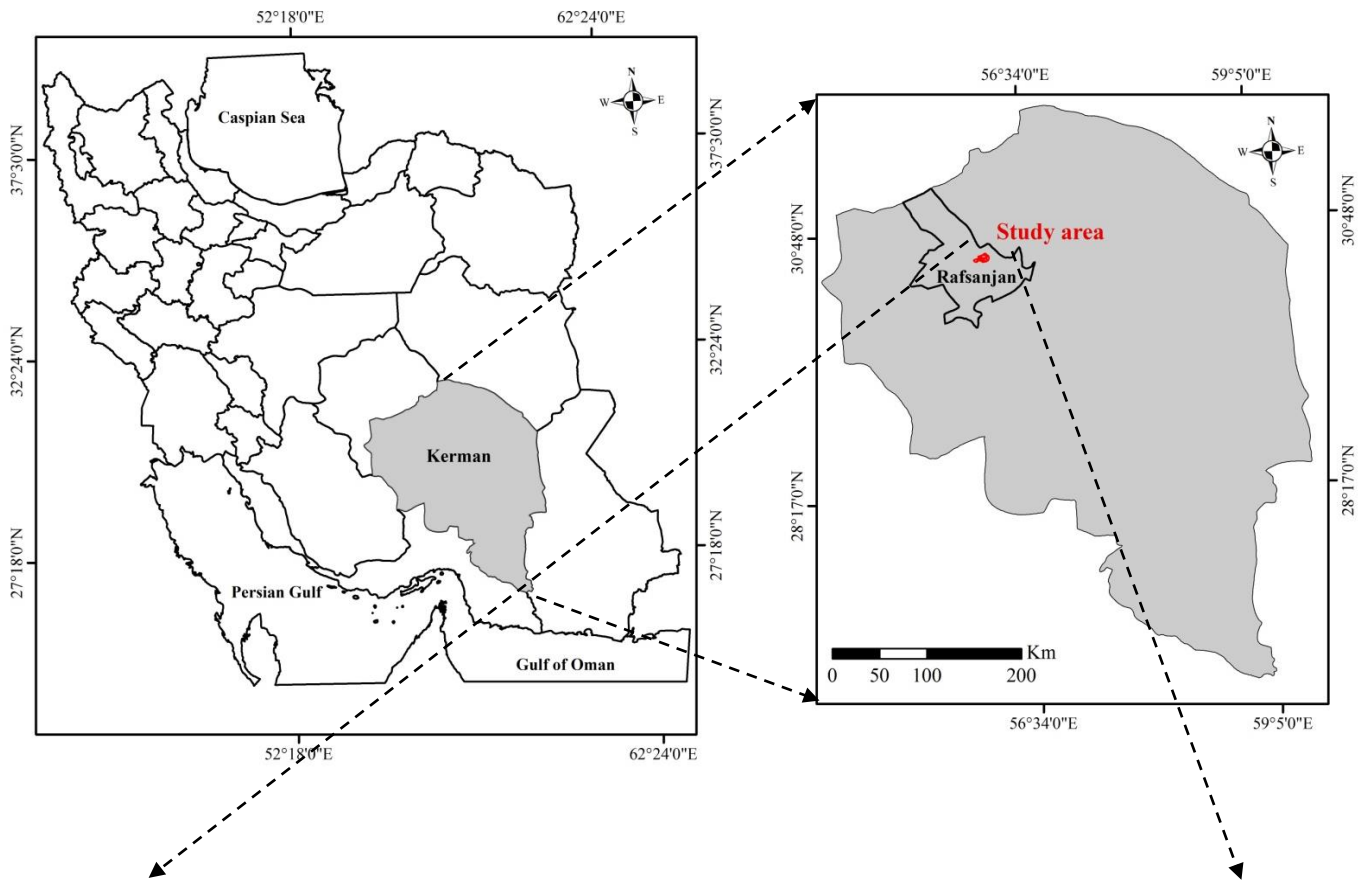


Figure 1. Location of the study are in Iran, Rafsanján region and Davaran area (Pe: pediment; Mfc: margin of fan and cultivated clay flat; Af: alluvial fan; Dp: desert pavement; Mps: margin of pediment and sand sheet; Ad: active drainage; Mfu: margin of fan and uncultivated clay flat)

Sample collection and laboratory analyses

Using the topographic map (1:25000 scale) and Google Earth satellite images, we identified and separated seven dominant geofoms of the region based on geopedological approach (Zinck, 1989), namely pediment (pedon 1: P1), margin of fan and cultivated clay flat (pedon 2: P2), alluvial fan (pedon 3: P3), desert pavement (pedon 4: P4), margin of pediment and sand sheet (pedon 5: P5), active drainage (pedon 6: P6), and margin of fan and uncultivated clay flat (pedon 7: P7).

According to the area of each geofom and based on fourth order surveys (Soil Science Division Staff, 2017), 19 pedons were excavated and described according to Schoeneberger et al. (2012). Subsequently, in each geofom, a representative pedon was selected (Fig. 1 and Table 1) and the soil samples were collected from different genetic horizons. Air-dried soil samples were crushed and passed through a 2-mm sieve. We carried out different soil physicochemical analyses, including soil organic carbon (OC) (Nelson and Sommers, 1982), particle size distribution (Gee and Bauder, 1986), calcium carbonate equivalent (CCE) (Nelson, 1982), gypsum (Nelson et al., 1978), soluble cations in saturation extract (Lanyon and Heald, 1982), pH in saturated paste, and electrical conductivity (EC) in saturated extract. In addition, the volume percentage of rock fragments (RF, greater than 2000 μm) and the weight percentage of sand fractions were determined by sieving, which included very fine sand (VFS, 50-100 μm), fine sand (FS, 100-250 μm), medium sand (MS, 250-500 μm), coarse sand (CS, 500-1000 μm), and very coarse sand (VCS, 1000-2000 μm).

The major elements of the soil samples were determined via an XRF-1800 sequential X-ray fluorescence spectrometer.

Chemical weathering indices

The weathering indices, including WIP, product index (PI), CIA, Silica-Sesquioxide Ratio (Kr), and CIA/WIP ratio (IR), were calculated using Equations (1) to (5) as follows:

$$\text{WIP} = \left[\left(\frac{2\text{Na}_2\text{O}}{0.35} \right) + \left(\frac{\text{MgO}}{0.9} \right) + \left(\frac{2\text{K}_2\text{O}}{0.25} \right) + \left(\frac{\text{CaO}}{0.7} \right) \right] \quad \text{Parker (1970)} \quad (1)$$

$$\text{PI} = \left[\left(\frac{\text{SiO}_2}{(\text{SiO}_2 + \text{TiO}_2 + \text{Al}_2\text{O}_3 + \text{Fe}_2\text{O}_3)} \right) \right] \times 100 \quad \text{Ruxton (1968)} \quad (2)$$

$$\text{CIA} = \left[\left(\frac{\text{Al}_2\text{O}_3}{(\text{Al}_2\text{O}_3 + \text{CaO} + \text{SiO}_2 + \text{Na}_2\text{O} + \text{K}_2\text{O})} \right) \right] \times 100 \quad \text{Nesbit \& Young (1982)} \quad (3)$$

$$\text{Kr} = \frac{\text{SiO}_2}{(\text{Al}_2\text{O}_3 + \text{Fe}_2\text{O}_3)} \quad \text{Moignien (1966)} \quad (4)$$

$$\text{IR} = \frac{\text{CIA}}{\text{WIP}} \quad \text{Garzanti et al. (2014)} \quad (5)$$

The amount of all the element oxides in these equations is in mole fraction. Moreover, the CaO in Equations (1) and (3) is the amount of CaO in the silicate minerals. Hence, the amount of calcium in carbonates (calcite and dolomite) and phosphates (apatite) was corrected using Equation (6), as follows:

$$\text{CaO}^* = 0.35 \times (2 \times \text{Na}_2\text{O})/62 \quad \text{Honda \& Shimizu (1998)} \quad (6)$$

Since the Al_2O_3 - $(\text{CaO}+\text{Na}_2\text{O})$ - K_2O (A-CN-K) ternary diagram is useful for indicating the chemical weathering trend (Nesbitt and Young, 1984; Fedo et al., 1997), the A-CN-K ternary diagrams were constructed with Triplot 2.1.4 software for different horizons of the studied pedons.

Detection of lithologic discontinuity (LD)

The uniformity value (UV) is an index that has been used successfully for the detection of LD (Cremeens and Mokma, 1986; Tsai and Chen, 2000). The UV index was calculated as:

$$UV = \frac{[(\% \text{silt} + \% \text{ very fine sand}) / (\% \text{sand} - \% \text{ very fine sand})] \text{ in upper horizon}}{[(\% \text{silt} + \% \text{ very fine sand}) / (\% \text{sand} - \% \text{ very fine sand})] \text{ in lower horizon}} - 1 \quad (7)$$

Results and Discussion

Soil physicochemical properties

Table 1 depicts the morphological characteristics and the most important physicochemical properties of the studied pedons. The pedons were classified based on the WRB soil classification system (IUSS Working Group WRB, 2015) (Table 2). The heterogeneity of the parent material (sequence of fluvial and aeolian sediments) was observed for most studied pedons. The single grain structure was the most dominant soil structure in the studied soils due to the presence of aeolian sediments in the majority of the pedons under study. Five reference soil groups (RSGs), including Calcisols, Gypsisols, Fluvisols, Solonchaks, and Regosols, were identified in the studied area (Table 2).

Detection of lithologic discontinuity

A great body of field evidence has indicated the presence of LDs, including an abrupt textural contact, the size of sand grain, the presence of stone lines, and the shape of rock fragments (Soil Taxonomy, 2014). In the present field study, all the pedons (except for P6, the active drainage geofom) exhibited LDs based on the differences concerning the type of the parent material (aeolian and fluvial sediments). The horizon sequence with LDs implied that the studied pedons were formed by cycling deposition of aeolian and fluvial sediments. According to Ahr *et al.* (2012), discontinuities are not always readily detectable in the field. Both laboratory analyses and field evidence are required to accurately distinguish LDs (Ahr *et al.*, 2012; Esfandiarpour-Boroujeni *et al.*, 2020).

Fig. 2 represents the depth functions of the clay-free sand fractions for the studied pedons. In P1, at depths of 70 cm (between the C and 2Cky horizons) and 105 cm (between the 2Cky and 3C horizons), all the fractions of the clay-free sand exhibited an abrupt change with depth (Fig. 2). The subsequent laboratory analyses confirmed the presence of LDs previously distinguished in the field (Tables 1 and 2). In P2, the vertical trend of MS to VFS fractions were in concordance with the field evidence. Despite the lack of a direct field evidence, the clay-free base of CS and VCS fractions revealed discontinuities at depths of 60 and 140 cm (Fig. 2).

Several studies have confirmed that the UV is a reliable index to detect LDs (Cremeens and Mokma, 1986; Tsai and Chen, 2000; Esfandiarpour-Boroujeni *et al.*, 2020). The UV index compares particle size data from two horizons. A UV index close to zero indicates that the two given horizons originate from similar parent materials. The UV values that exceed ± 0.6 suggest that an LD exists between these two horizons. In the present study, the UV values were zero for the depths of 60 and 140 cm of the P2, failing to reveal any LDs between the 2Bky-2C1 and 2C1-2C2 horizons (Fig. 3). Accordingly, distinguishing LDs necessitates a combination of the laboratory analyses and field evidence. In the alluvial fan geofom (P3), field evidence, depth functions of the clay-free sand fractions, and the UV values revealed the presence of the LDs (Table 2 and Figs. 2 and 3).

Table 1. Summary of the morphological characteristics of the studied pedons^a

Horizon	Depth (cm)	Type of sediment	Boundary	Color		Structure	Consistency		Cutans and/or concentrations
				Dry	Moist		Dry	Moist	
Pedon 1 (Pediment)									
C	0-70	Aeolian	AW	10YR 6/4	10YR 5/3	sg	lo	lo	
2Cky	70-105	Fluvial	CW	10YR 7/4	10YR 6/2	sg	sh	vfr	f,1,CAC and GYX,MAT
3C	105-200	Aeolian	AS	10YR 6/4	10YR 5/3	sg	sh	vfr	
Pedon 2 (Margin of fan and cultivated clay flat)									
C	0-30	Aeolian	AS	7/5YR 6/4	7/5YR 5/2	sg	lo	lo	
2Bky	30-60	Fluvial	CW	10YR 7/4	10YR 6/2	1fsbk	sh	fi	f,1,CAC and GYX,MAT
2C1	60-140	Fluvial	AS	10YR 6/4	10YR 5/2	m	mh	fi	
2C2	140-160	Fluvial	CS	10YR 6/4	10YR 5/2	sg	sh	fi	
3Btn	160-205	Aeolian	AS	10YR 5/4	10YR 4/4	1fsbk	mh	fi	f, F, CLF on PF
Pedon 3 (Alluvial fan)									
C	0-25	Aeolian	CS	10YR 6/4	10YR 5/3	sg	lo	lo	
2BK	25-60	Fluvial	CW	10YR 7/4	10YR 6/3	1fsbk	sh	vfi	c,2,CAC,MAT
3By	60-110	Aeolian	CS	10YR 7/4	10YR 6/3	sg	sh	vfi	f,1,GYX,MAT
4C1	110-130	Fluvial	CS	10YR 6/4	10YR 5/3	m	mh	fi	
4C2	130-175	Fluvial	AS	10YR 6/4	10YR 5/3	m	mh	fi	
Pedon 4 (Desert pavement)									
C	0-20	Aeolian	CS	10YR 6/4	10YR 5/3	sg	lo	lo	
2Bw	20-50	Fluvial	AS	7/5YR 6/4	7/5YR 5/3	1fsbk	sh	vfi	
3Bky	50-105	Aeolian	AS	10YR 7/4	10YR 5/3	1fsbk	sh	vfi	f,1,CAC and GYX,MAT
3Ck	105-125	Aeolian	AS	10YR 6/4	10YR 5/3	sg	mh	fi	f,1,CAC,MAT
4CBy	125-180	Fluvial	CW	10YR 7/4	10YR 5/3	sg	mh	fi	f,1,GYX,MAT
4Cy	180-220	Fluvial	AS	10YR 8/3	10YR 6/3	m	h	vfi	f,1,GYX,TOT
Pedon 5 (Margin of pediment and sand sheet)									
C	0-15	Aeolian	AS	10YR 6/4	10YR 5/3	sg	lo	lo	
CBk	15-45	Aeolian	AS	10YR 5/4	10YR 4/3	sg	lo	lo	f,1,CAC,MAT
Ck	45-60	Aeolian	AS	10YR 6/4	10YR 5/3	sg	lo	lo	f,1,CAC,MAT
2C1	60-75	Fluvial	AW	10YR 6/4	10YR 5/3	sg	lo	lo	
2C2	75-95	Fluvial	AW	10YR 6/4	10YR 5/3	sg	lo	lo	
3C3	95-105	Aeolian	AW	10YR 6/4	10YR 5/3	sg	lo	lo	
3C4	105-115	Aeolian	AW	10YR 5/4	10YR 4/3	sg	lo	lo	
3C5	115-125	Aeolian	AW	10YR 6/4	10YR 5/3	sg	lo	lo	
4Ck	125-140	Fluvial	AW	10YR 6/4	10YR 5/3	sg	lo	lo	f,1,CAC,MAT
4Bky	140-215	Fluvial	AS	10YR 7/4	10YR 6/3	1fabk	sh	fi	c,1,CAC,MAT and f,1,GYX,MAT

Continued Table 1. Summary of the morphological characteristics of the studied pedons^a

									Pedon 6 (Active drainage)		
C1	0-55	Fluvial	AS	10YR 6/4	10YR 5/3	m	h	vfi			
C2	55-85	Fluvial	AS	10YR 6/4	10YR 5/3	m	h	vfi			
C3	85-200	Fluvial	AS	10YR 6/4	10YR 5/3	m	h	vfi			
									Pedon 7 (Margin of fan and uncultivated clay flat)		
C	0-60	Aeolian	AS	10YR 7/4	10YR 6/4	sg	lo	lo			
2Bwb1	60-100	Fluvial	AS	10YR 6/4	10YR 5/3	1fsbk	mh	fi			
2Bwb2	100-140	Fluvial	AS	10YR 6/4	10YR 5/3	2fsbk	mh	fi			
2Bzb	140-200	Fluvial	Aw	10YR 7/4	10YR 6/3	1msbk	mh	fi			m,2,SAX,MAT
3Bwb1	200-250	Aeolian	AS	10YR 6/4	10YR 5/3	1fsbk	mh	fi			
3Bwb2	250-310	Aeolian	AS	10YR 6/4	10YR 5/3	2fsbk	mh	fi			
3Btb	310-350	Aeolian	AS	10YR 6/4	10YR 5/3	2msbk	mh	fi			f, F, CLF on CC
4Bwb	350-390	Fluvial	AS	10YR 6/4	10YR 5/3	1fsbk	mh	fi			

^a Symbols are used based on Schoeneberger et al. (2012) as follows:

Boundary — A: abrupt; W: wavy; S: smooth; C: clear.

Structure grade — 1: weak; 2: moderate.

Structure size — f: fine; m: medium.

Structure type — sg: single grain; m: massive; abk: angular blocky; sbk: subangular blocky.

Consistency — lo: loose; sh: slightly hard; mh: moderately hard; h: hard; vfr: very friable; fi: firm; vfi: very firm.

Cutans — f: few; F: faint distinctness; CLF: clay films (argillans); CC: on concretions; PF: on all faces of peds (vertical and horizontal).

Concentrations — f: few, c: common; m: many quantities; 1: fine size; 2: medium size; CAC: carbonate concretions; GYX: gypsum crystals; SAX: salt crystals; MAT: in the matrix (not associated with peds/pores); TOT: throughout.

Table 2. Summary of the physical and chemical properties of the studied pedons with their classification based on the WRB system

Horizon	Depth (cm)	pH	EC ^a (dS m ⁻¹)	Sand (%)	Silt (%)	Clay (%)	Textural class ^b	CCE ^c (%)	Gypsum (%)	OC ^d (%)	SAR ^e (mmol l ⁻¹) ^{0.5}	CF ^f (>2 mm)
Pedon 1 (Pediment): Haplic Gypsisols (Arenic, Aridic, Hypogypsic, Raptic, Protosodic)												
C	0-70	7.64	1.94	86.60	9.4	4	LS	3.0	0.0	0.01	1.27	0.0
2Cky	70-105	7.78	2.89	85.80	5.7	8.5	LS	14.5	8.9	0.01	7.80	10.0
3C	105-190	8.09	4.20	89.24	6.5	4.3	S	12.5	0.0	0.01	15.24	3.0
Pedon 2 (Margin of fan and cultivated clay flat): Calcic Solonchaks (Aridic, Calcaric, Loamic, Raptic)												
C	0-30	7.29	16.08	47.50	32	20.5	L	12.5	0.0	0.09	3.39	10.0
2Bky	30-60	7.68	18.20	27.50	56	16.5	SiL	17.5	1.8	0.07	2.31	5.0
2C1	60-140	7.69	22.90	30.00	54.5	15.5	SiL	12.0	0.0	0.06	1.94	7.0
2C2	140-160	7.58	12.84	28.50	52	19.5	SiL	2.6	0.0	0.05	3.28	20.0
3Btn	160-205	7.82	16.20	44.50	29	26.5	L	10.0	0.0	0.02	17.89	10.0
Pedon 3 (Alluvial fan): Haplic Calcisols (Aridic, Fluvic, Loamic, Raptic)												
C	0-25	7.80	0.68	68.50	21	10.5	SL	2.7	0.0	0.01	3.48	20.0
2BK	25-60	7.62	2.64	63.30	10.7	26	SCL	30.0	0.0	0.01	2.81	30.0
3By	60-110	7.50	6.16	72.70	10.1	20.5	SCL	20.0	2.3	0.01	4.99	25.0
4C1	110-130	8.20	7.04	82.30	9.3	8.5	LS	18.5	1.4	0.01	7.91	90.0
4C2	130-175	7.66	6.23	85.00	9	6	LS	16.4	0.0	0.01	5.99	75.0
Pedon 4 (Desert pavement): Cambic Calcisols (Fluvic, Loamic, Raptic, Yermic)												
C	0-20	8.00	0.12	85.50	4	10.5	LS	7.0	0.0	0.05	0.93	10.0
2Bw	20-50	8.06	11.0	73.00	5	22	SCL	12.5	0.0	0.05	3.74	20.0
3Bky	50-105	7.76	10.66	73.50	16	10.5	SL	32.5	1.4	0.04	2.44	30.0
3Ck	105-125	8.24	9.60	77.50	12	10.5	SL	9.0	0.0	0.04	4.86	80.0
4CBy	125-180	8.00	6.67	69.50	24.5	6	SL	9.0	5.5	0.03	13.86	85.0
4Cy	180-220	7.97	10.98	75.50	16.0	8.5	SL	7.5	6.3	0.03	15.03	40.0
Pedon 5 (Margin of pediment and sand sheet): Skeletic Calcisols (Arenic, Aridic, Fluvic, Raptic, Protosodic)												
C	0-15	7.82	0.09	93.50	2	4.5	S	2.5	0.0	0.01	2.20	0.0
CBk	15-45	7.81	2.21	75.50	12	12.5	SL	26.0	0.0	0.23	6.19	49.7
Ck	45-60	7.90	3.65	88.50	6.25	5.25	S	5.0	0.0	0.05	10.14	53.5
2C1	60-75	8.09	2.13	90.80	4.7	4.5	S	15.0	0.0	0.04	7.84	18.8
2C2	75-95	8.38	2.23	91.40	4.5	4.1	S	12.5	0.0	0.03	9.80	52.4
3C3	95-105	8.42	2.12	89.50	6	4.5	S	16.0	0.0	0.03	7.68	13.8
3C4	105-115	8.20	5.45	89.00	7.4	3.6	S	27.5	0.0	0.02	5.14	85.5
3C5	115-125	8.13	5.65	88.90	7.1	4	S	26.5	0.0	0.01	1.67	26.7
4Ck	125-140	8.02	5.74	80.00	15	5	LS	24.5	0.0	0.01	1.40	44.6
4Bky	140-215	7.80	8.78	77.00	18	5	LS	15.0	4.4	0.01	16.33	35.9

Continued Table 2. Summary of the physical and chemical properties of the studied pedons with their classification based on the WRB system

Pedon 6 (Active drainage): Calcaric Skeletic Fluvisols (Arenic, Aridic)												
C1	0-55	7.88	1.59	73.50	20	6.5	SL	22.5	0.0	0.05	1.25	72.4
C2	55-85	7.85	1.18	79.54	15	5.5	LS	18.0	0.0	0.01	2.44	83.1
C3	85-200	7.77	6.46	80.54	12	7.5	LS	15.0	0.0	0.04	6.63	87.0
Pedon 7 (Margin of fan and uncultivated clay flat): Protic Calcaric Eutric Regosols (Aeolic, Aridic, Loamic, Magnesic, Nechic, Transportic) over Calcic Sodic Solonchaks (Aridic, Clayic, Hypersalic, Skeletic)												
C	0-60	8.33	2.00	79.50	11	9.5	SL	7.5	0.0	0.01	2.03	0.0
2Bwb1	60-100	7.67	20.70	33.50	18	48.5	C	20.0	0.0	0.03	3.39	53.5
2Bwb2	100-140	7.32	23.40	31.25	17	51.75	C	27.5	0.0	0.02	6.01	51.1
2Bzb	140-200	7.83	63.20	29.50	20	50.5	C	10.0	0.0	0.02	4.13	48.5
3Bwb1	200-250	7.68	18.80	25.50	18	56.5	C	28.5	0.0	0.02	4.42	53.5
3Bwb2	250-310	7.92	16.80	25.00	20	55	C	22.5	0.0	0.01	3.78	42.5
3Btb	310-350	7.13	17.42	15.50	12.5	72	C	18.5	0.0	0.02	1.16	51.4
4Bwb	350-390	7.23	19.15	18.00	26	56	C	25.0	0.0	0.01	1.49	55.4

^a Electrical conductivity^b S = sandy, LS = loamy sandy, L = loam, SiL = silt loam, SL = sandy loam, SCL = sandy clay loam, C = clay.^c Calcium carbonate equivalent^d Organic carbon^e Sodium adsorption ratio^f Coarse fragments

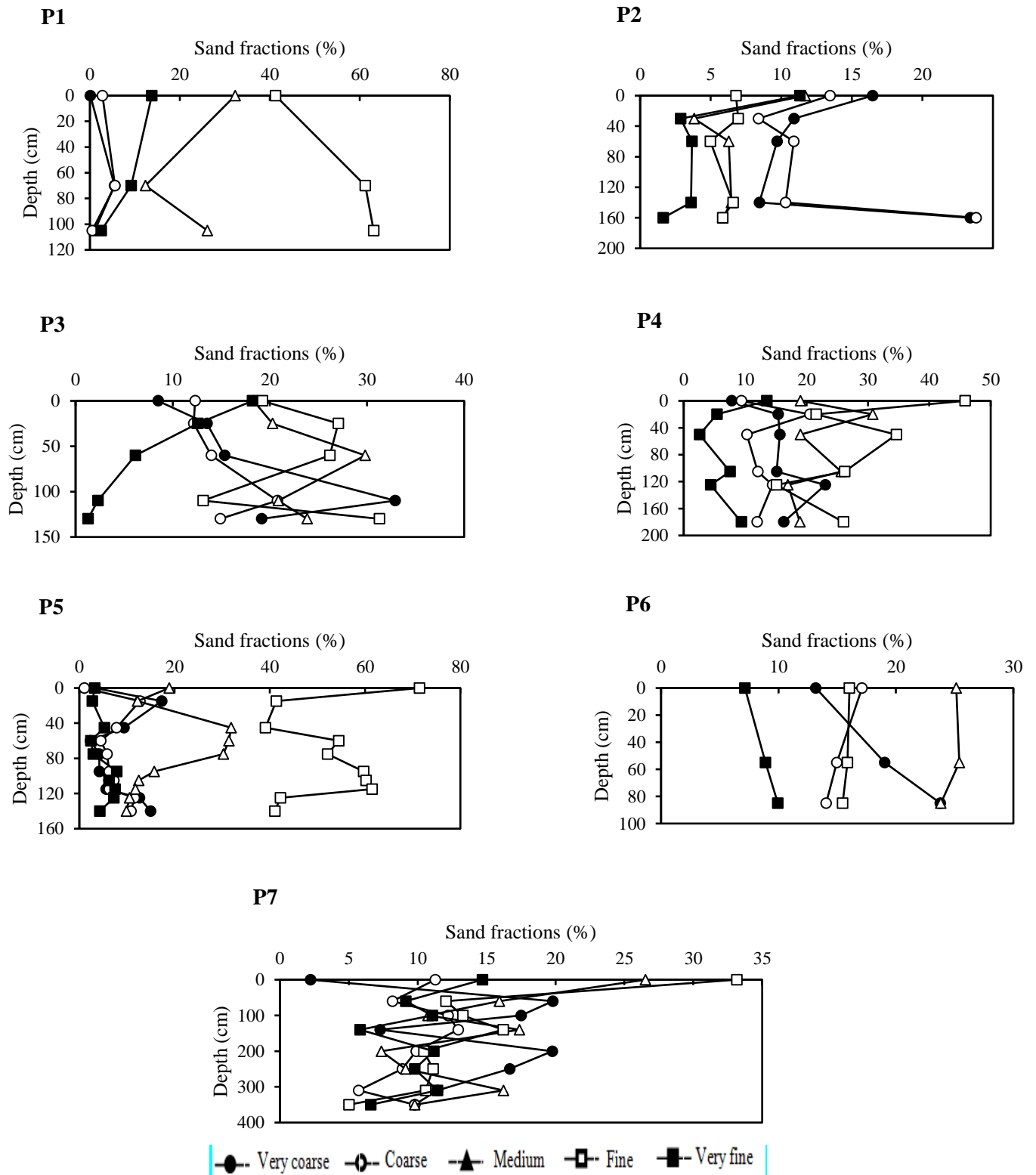


Figure 2. Depth function of various clay-free sand fractions for the studied pedons

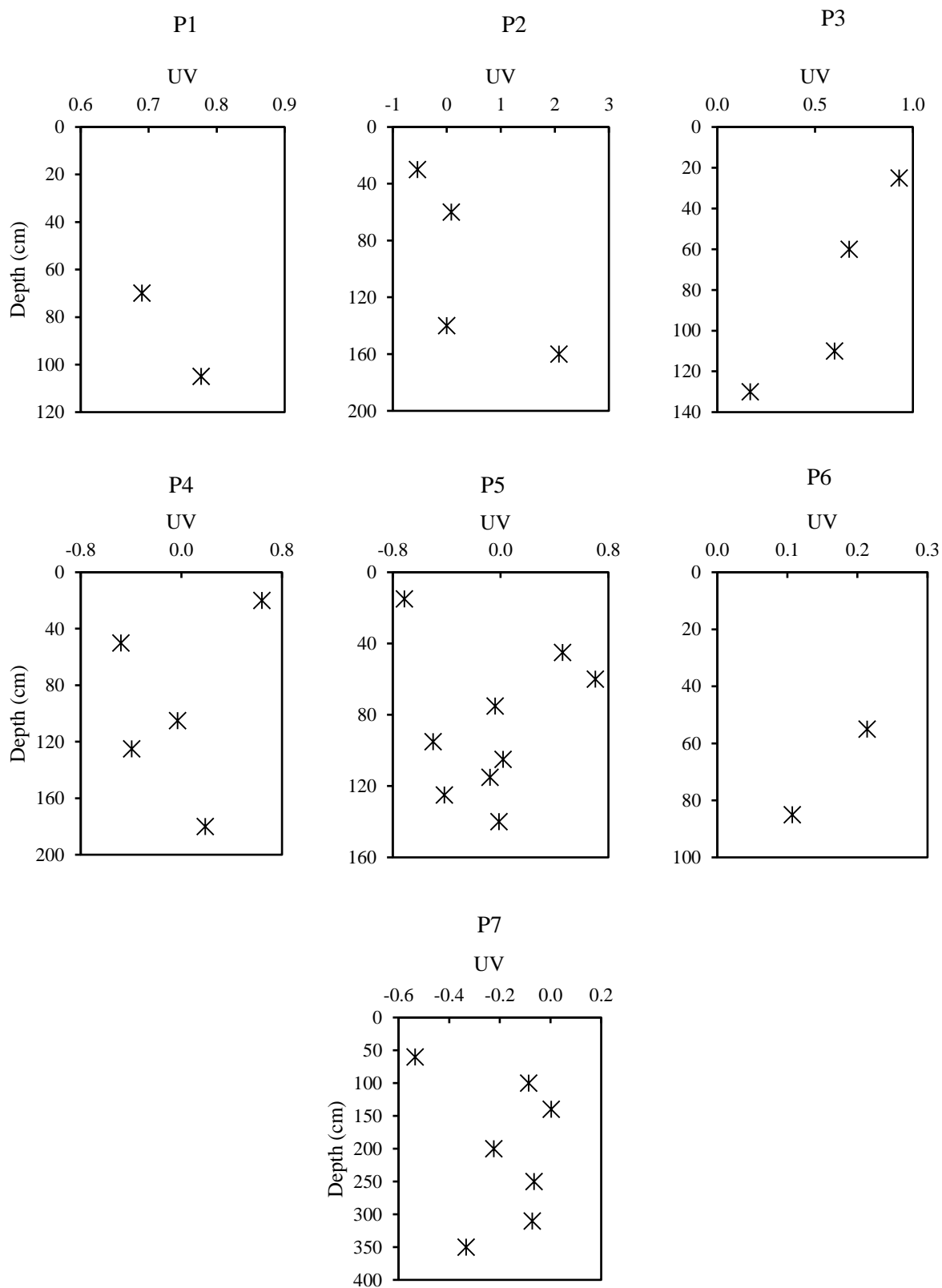


Figure 3. The uniformity value (UV) index of the studied pedons

The field evidence, values of the UV index, and the depth functions of all the clay-free base sand fractions showed LDs between C-2Bw and 2Bw-3Bky horizons in P4 (Table 2 and Figs. 2 and 3). Moreover, the clay-free base FS and VCS fractions were in line with the UV values and field evidence, showing an LD at depth of 125 cm in this pedon (Table 2 and Figs. 2 and 3). In P5, field evidence, depth functions of clay-free sand fractions (VCS, FS, and VFS), along with the values of the UV index demonstrated the heterogeneity of parent material at depths of 60, 95, and 125 cm, respectively (Table 2 and Figs. 2 and 3). The clay-free base of some sand fractions (MS and CS) exhibited an abrupt change at depths of 15 and 45 cm (Fig. 2). In conformation with the field evidence, none of the clay-free sand fractions revealed discontinuities between horizons in P6, which suggested that these horizons may be of the same origin. Furthermore, the field evidence, values of the UV index, and depth functions of the clay-free base sand fractions showed LDs among C-2Bwb1, 2Bzb-3Bwb1, and 3Btb-4Bwb horizons in P7 (Table 2 and Figs. 2 and 3).

Depth distribution of the weathering indices

Table 3 enlists the major oxide concentrations for different horizons of the studied pedons. The depth distribution of the weathering indices of WIP, IR, PI, and Kr are presented in Fig. 4. The WIP index values showed an irregular pattern with depth for all the studied pedons, except for P1 and P6. In P1, the values of WIP decreased with depth whereas an increasing trend was observed in P6 (Fig. 4). Although the values of PI and Kr indices decreased with depth in P1 and P2, they gradually increased in P6. The values of PI and Kr indices had irregular trends in the other studied pedons (Fig. 4). Moreover, the depth-related variations in the IR index revealed an irregular trend for all the pedons, except for P6.

These vertical variations confirmed the heterogeneity of parent material in the studied soils. According to Okewale (2020), the weathering progresses steadily with depth for homogenous rocks along a vertical profile whereas a contrast may be found for heterogeneous rocks from different locations and formations. Based on the steep reverse trend of chemical proxy of alteration (CPA) and index B, Vasu et al. (2020) identified the presence of the LD in pedons and demonstrated that the parent materials of the studied pedons were of different origins.

As mentioned above, no LD was detected in P6, which was confirmed by the lack of field evidence and the results of the laboratory analyses. In this pedon, the depth distribution of the weathering indices were completely different from those on the other pedons (increasing steadily) and the weathering intensity decreased with depth. On the other hand, several studies have reported that the variation in chemical weathering values commonly reflects variation in grain sizes rather than the extent of the chemical weathering (Nesbitt and Young, 1982; Hatano et al., 2019). Hatano et al. (2019) and Guo et al. (2018) proposed that the Al_2O_3/SiO_2 ratio is an appropriate grain size index. Fig. 5 illustrates the vertical change of Al_2O_3/SiO_2 ratio for different studied pedons. The variability of Al_2O_3/SiO_2 ratio along a vertical profile is in complete agreement with the depth distribution of the chemical weathering indices. In P6, the Al_2O_3/SiO_2 ratio decreased with depth, confirming the vertical change of the weathering indices. Quartz is resistant to chemical and physical weathering and coarse-grained sediments are enriched in quartz and possess high SiO_2 contents. In contrast, fine-grained sediments are commonly enriched in phyllosilicates with high Al_2O_3 contents (Nesbitt et al., 1996; Carpentier et al., 2009; Lupker et al., 2012).

Table 3. Some of the major oxide elements of the studied pedons

Horizon	Depth (cm)	TiO ₂	SiO ₂	Fe ₂ O ₃	Na ₂ O	MgO	K ₂ O	CaO	Al ₂ O ₃
		%							
Pedon 1 (Pediment)									
C	0-70	1.06	39.96	13.87	0.32	6.46	5.08	18.82	13.05
2Cky	70-105	1.07	40.11	13.23	0.40	6.37	4.73	19.22	13.28
3C	105-200	1.34	35.33	18.43	0.47	6.05	4.72	18.90	13.08
Pedon 2 (Margin of fan and cultivated clay flat)									
C	0-30	1.02	44.51	8.88	0.71	6.11	5.40	16.36	15.59
2Bky	30-60	1.54	34.65	13.52	0.61	7.40	6.35	19.91	14.34
2C1	60-140	1.48	35.40	13.17	1.19	6.53	6.16	19.57	14.80
2C2	140-160	1.27	37.94	13.64	0.34	5.72	5.13	19.27	15.30
3Btn	160-205	1.38	34.25	15.41	0.52	5.77	6.10	19.51	15.31
Pedon 3 (Alluvial fan)									
C	0-25	1.15	36.02	17.55	0.34	5.25	5.34	19.14	13.47
2BK	25-60	1.13	36.36	10.66	0.31	7.65	6.10	20.45	15.62
3By	60-110	1.03	38.02	9.86	0.43	7.30	5.48	21.38	14.78
4C1	110-130	1.05	30.44	20.81	0.38	9.62	5.18	19.26	11.57
4C2	130-175	1.00	38.60	19.00	0.41	9.52	4	32.99	13.17
Pedon 4 (Desert pavement)									
C	0-20	1.37	35.98	16.06	0.32	6.46	5.28	19.49	13.48
2Bw	20-50	1.24	36.79	9.66	0.38	11.11	4.85	20.15	14.23
3Bky	50-105	1.16	36.66	2.70	0.37	18.36	4.79	20.82	13.59
3Ck	105-125	1.19	39.19	14.67	0.35	5.53	5.45	18.95	13.11
4CBy	125-180	1.17	37.86	13.92	0.53	6.63	4.78	20.69	12.92
4Cy	180-220	0.96	39.66	8.10	0.60	8.13	6.29	21.49	13.34
Pedon 5 (Margin of pediment and sand sheet)									
C	0-15	1.16	39.30	13.55	0.33	5.90	5.13	19.49	13.45
CBk	15-45	1.03	39.08	13.32	0.38	6.27	5.24	19.29	13.72
Ck	45-60	1.30	36.62	17.94	0.39	5.25	5.08	18.82	13.11
2C1	60-75	1.05	40.36	13.86	0.38	5.98	5.24	18.62	13.00
2C2	75-95	1.23	38.76	15.23	0.40	5.58	5.08	18.81	13.26
3C3	95-105	1.14	36.32	17.28	0.39	5.53	5.03	19.49	13.34
3C4	105-115	1.25	38.62	13.32	0.38	7.76	5.00	18.95	13.22
3C5	115-125	1.10	39.53	13.87	0.33	5.72	4.95	19.62	13.43
4Ck	125-140	1.02	40.26	11.62	0.32	6.83	4.79	20.49	13.11
4Bky	140-215	1.07	39.23	11.09	0.56	4.88	6.29	21.56	13.77
Pedon 6 (Active drainage)									
C1	0-55	1.13	38.18	33.01	0.32	6.46	5.43	20.82	14.16
C2	55-85	1.08	39.65	32.09	0.35	7.39	4.80	21.49	13.34
C3	85-200	1.10	38.93	27.38	0.47	11.85	5.18	22.42	13.75
Pedon 7 (Margin of fan and uncultivated clay flat)									
C	0-60	1.30	36.61	15.74	0.33	6.46	5.08	18.82	13.93
2Bwb1	60-100	1.31	38.61	1.30	0.36	6.83	12.91	20.15	16.78
2Bwb2	100-140	1.05	39.53	10.66	0.38	6.39	7.14	19.33	13.99

2Bzb	140-200	1.29	35.73	10.37	0.39	9.49	7.35	19.82	13.96
3Bwb1	200-250	1.11	39.47	9.58	0.37	7.39	7.38	19.16	14.00
3Bwb2	250-310	1.10	39.59	8.18	0.33	7.31	6.08	21.29	14.57
3Btb	310-350	1.26	39.53	7.28	0.32	5.57	6.50	22.90	15.03
4Bwb	350-390	1.25	40.08	5.17	0.30	9.92	7.49	20.15	14.13

Qin and Mu (2011) demonstrated that the abundances of Al_2O_3 , Fe_2O_3 , K_2O , MnO , P_2O_5 , and MgO contents in fine grain fractions are higher than those in coarse grain fractions, and that SiO_2 , Na_2O , and CaO contents in the fine grain fractions are lower than those in the coarse grain fractions. Hatano et al. (2019) reported a strong positive correlation between the chemical weathering and grain size index and established that the CIA value is greatly controlled by the grain size. However, according to Vasu et al. (2020), the effects of the grain size on the weathering indices and variation in sediments complicate the assessment of the chemical weathering degree.

Our results revealed that the vertical trend of $\text{Al}_2\text{O}_3/\text{SiO}_2$ ratio is closely matched with the presence of LDs. The horizons with lower $\text{Al}_2\text{O}_3/\text{SiO}_2$ ratio suggested that these samples were composed of coarser grained sediments. Fig. 6 exhibits the correlation matrix between the $\text{Al}_2\text{O}_3/\text{SiO}_2$ ratio and particles size. The sand, FS, and MS fractions were negatively correlated ($P \leq 0.05$) with the grain size index ($\text{Al}_2\text{O}_3/\text{SiO}_2$ ratio) while the clay and silt fractions were positively correlated with the $\text{Al}_2\text{O}_3/\text{SiO}_2$ ratio (Fig. 6). These results also shed light on the effect of the grain size on the variation of $\text{Al}_2\text{O}_3/\text{SiO}_2$ ratio. Where LDs were present, an abrupt change of $\text{Al}_2\text{O}_3/\text{SiO}_2$ ratio was observed between the horizons (Fig. 5). The sharp vertical changes in $\text{Al}_2\text{O}_3/\text{SiO}_2$ ratio were due to the presence of an LD.

The variation in the chemical weathering values between the horizons with different $\text{Al}_2\text{O}_3/\text{SiO}_2$ ratios reflected distinctive differences in terms of the parent material. We could accordingly propose that the $\text{Al}_2\text{O}_3/\text{SiO}_2$ ratio and chemical weathering indices are reliable indicators of the presence of LDs (a quantitative method). On the other hand, assessment of the grain size is of great necessity for the evaluation and interception of the vertical trend of weathering indices, especially where sediments have variable grain sizes and are formed on different sedimentary cycles.

In P6, the effects of the sedimentary recycling and hydraulic sorting on the chemical weathering indices were evident. Despite the lack of LD in this pedon, there was an abrupt change in the chemical weathering indices, such as WIP and IR, at a depth of 55 cm, which was further confirmed by the $\text{Al}_2\text{O}_3/\text{SiO}_2$ ratio. Among the studied pedons, P6 was the only pedon formed entirely from fluvial sediments. In the fluvial sediments, hydrodynamic sorting can separate particles according to their size, shape, and density, thereby controlling the mineralogical variability as well as geochemical differentiation in river sediments (Garzanti et al., 2010 and 2011). Therefore, in pedon P6, the vertical variation of the chemical weathering indices can reflect the effects of sedimentary recycling and sorting during the sediment transportation and deposition. These results collectively suggested that different factors, such as grain size, sedimentary recycling, and their interactive effects, should be considered for chemical weathering assessment. Guo et al. (2018) investigated the effect of sorting on river sediment geochemical composition and weathering indices in five rivers in the east of China. Their results showed that the weathering intensity in the fine-grained particles was systemically stronger than that in the coarse-grained particles.

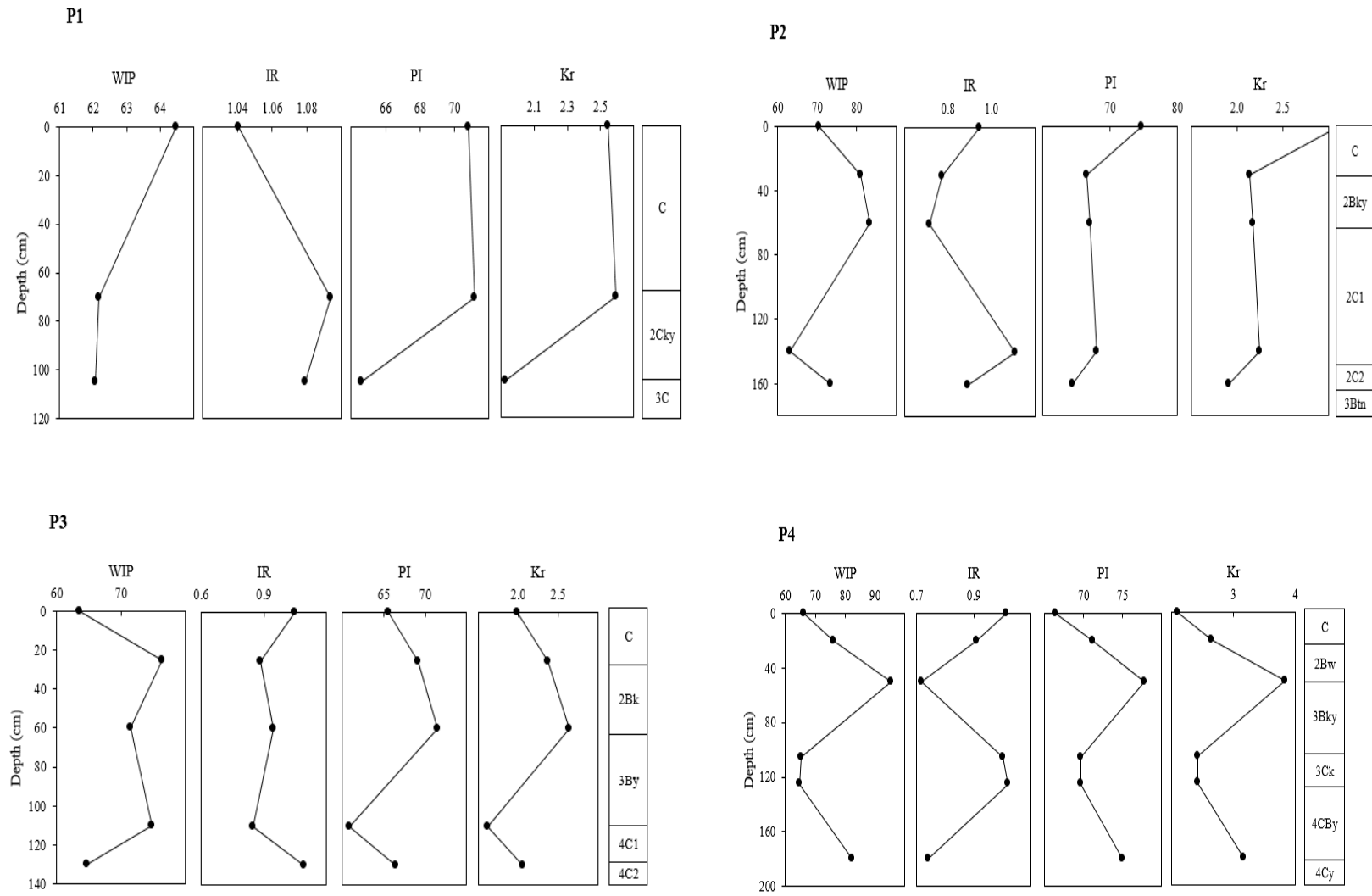
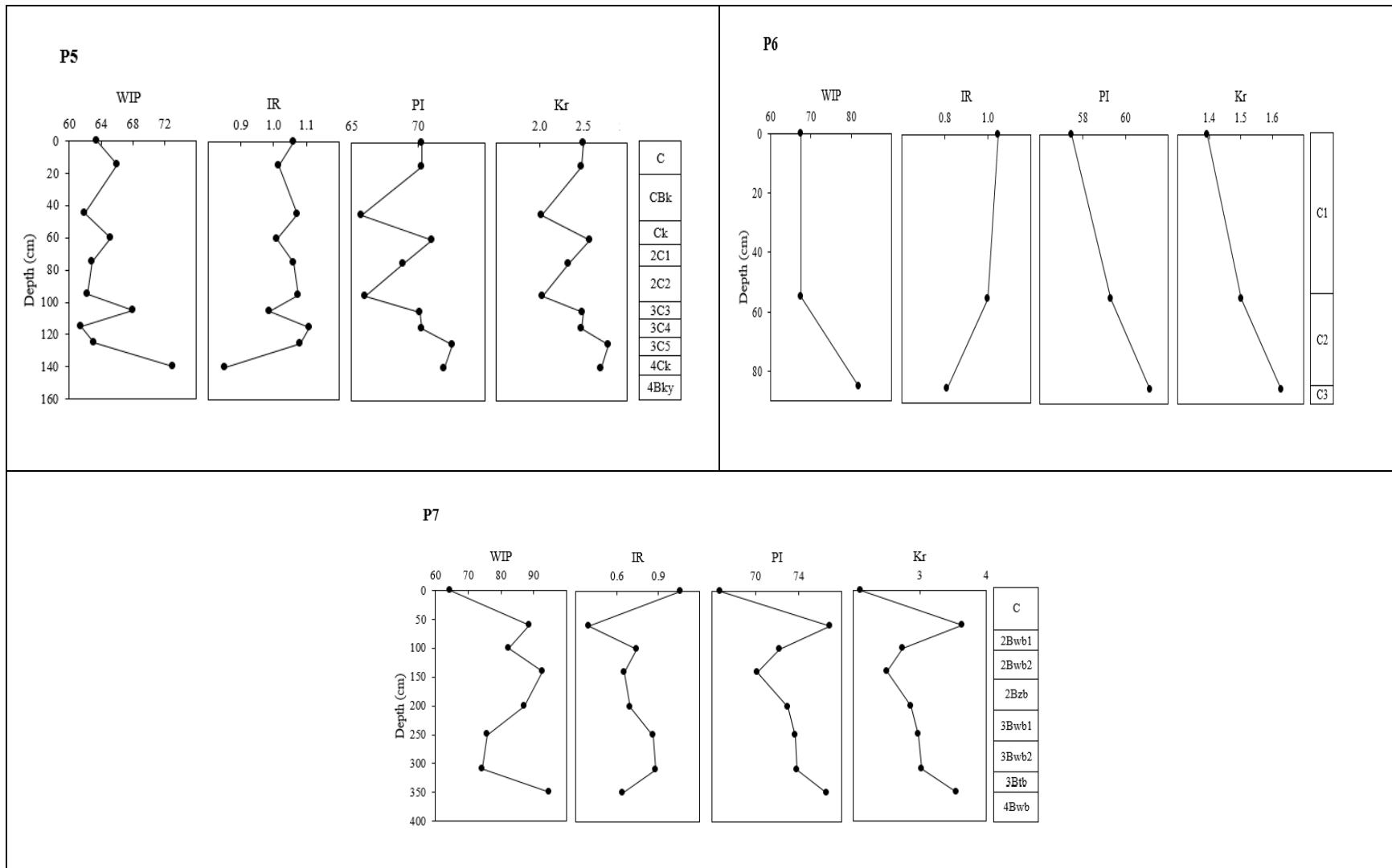


Figure 4. Depth distributions of weathering indices for the studied pedons



Continued Figure 4. Depth distributions of weathering indices for the studied pedons

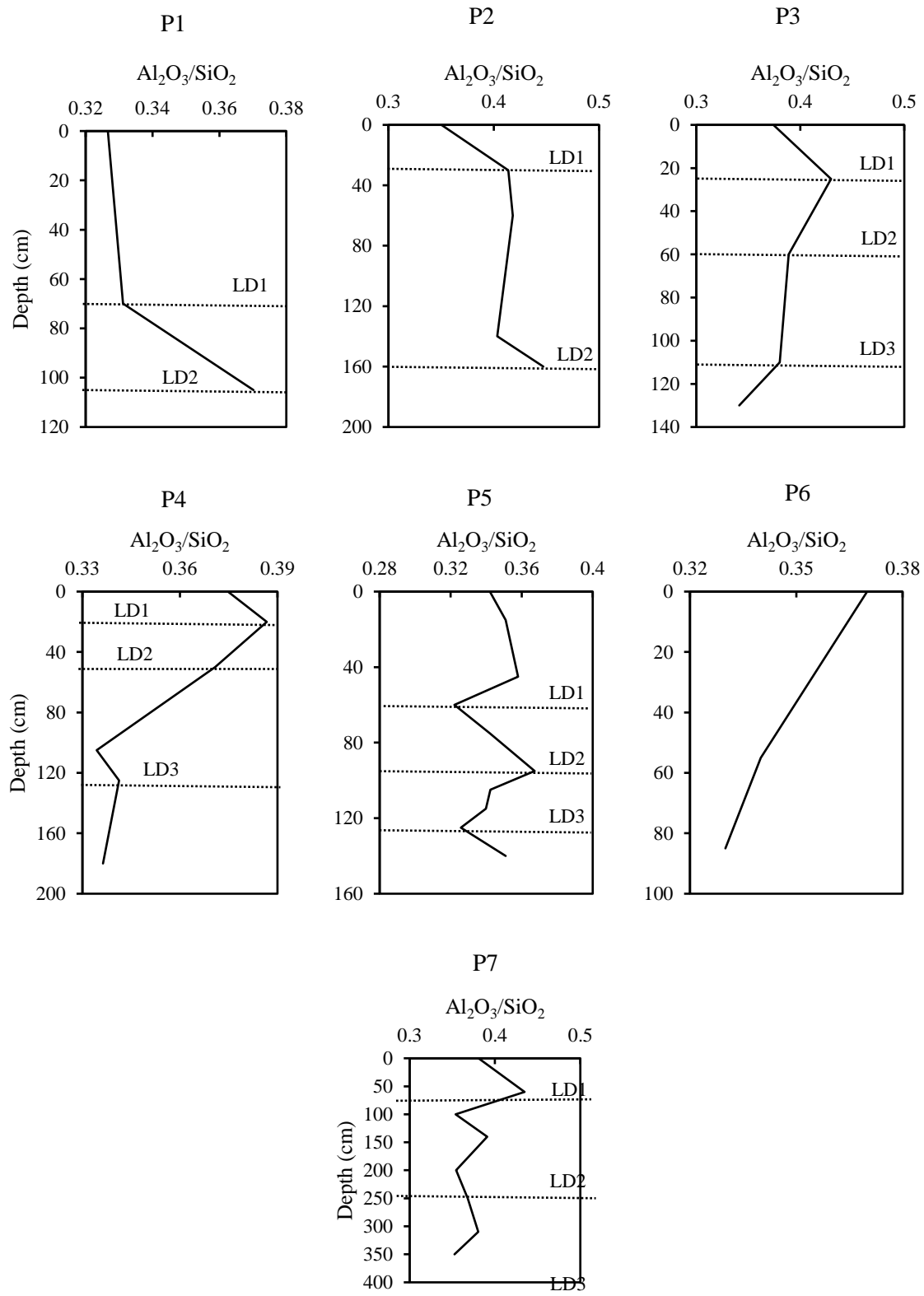


Figure 5. Vertical trend of $\text{Al}_2\text{O}_3/\text{SiO}_2$ ratio for the studied pedons (LD: lithologic discontinuity)

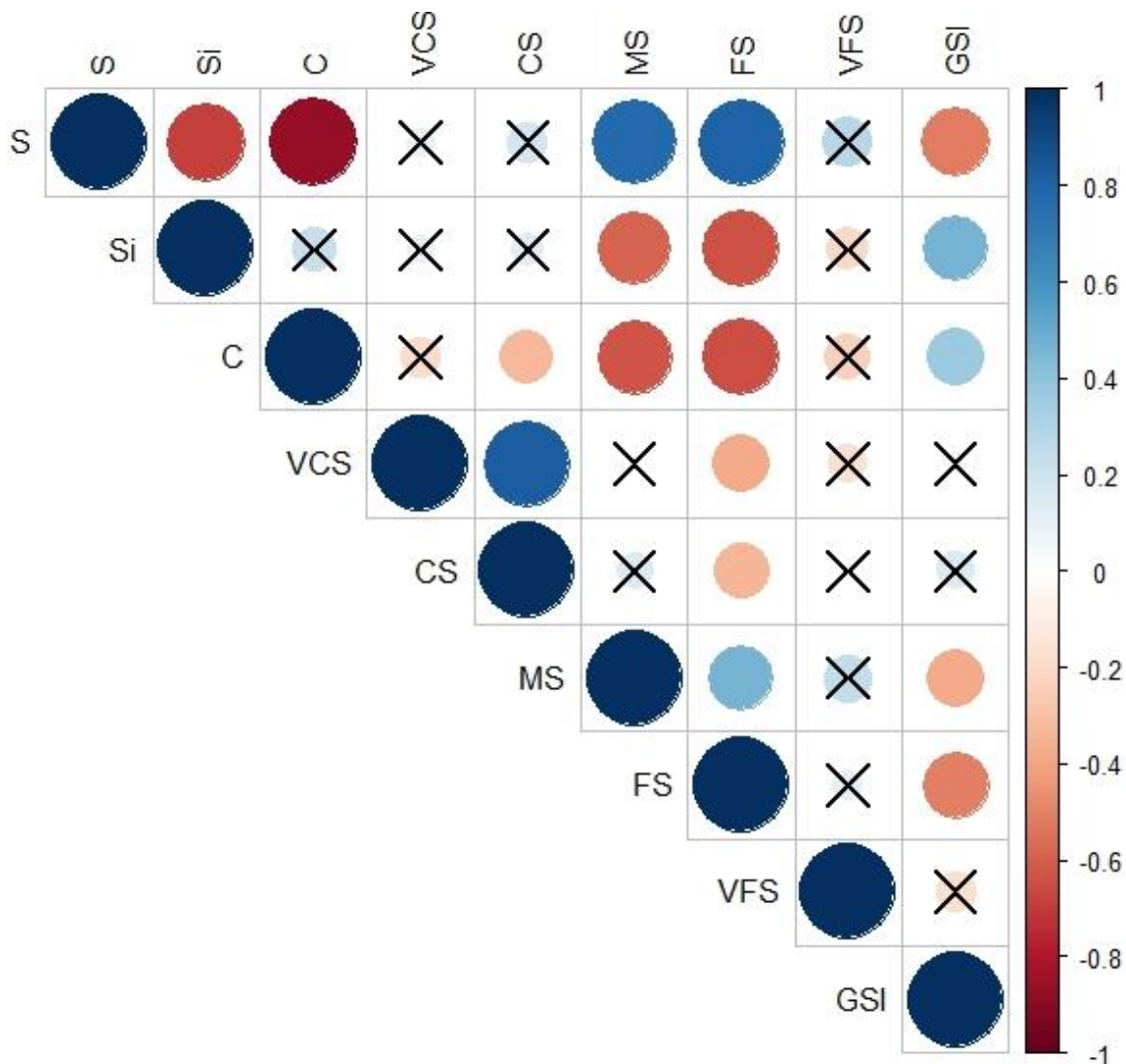


Fig. 6. Correlation matrix among $\text{Al}_2\text{O}_3/\text{SiO}_2$ ratio and particle size (S: sand; Si: silt; C: clay; VCS: very coarse sand; CS: coarse sand; MS: medium sand; FS: fine sand; VFS: very fine sand; GSI: grain size index ($\text{Al}_2\text{O}_3/\text{SiO}_2$ ratio); level of significance is 0.05 and for insignificant correlations, coefficient crosses were added).

The A-CN-K ternary diagram is a useful indicator of the chemical weathering trend (Nesbitt and Young, 1984; Fedo et al., 1997). The studied pedons and their horizons were plotted on the A-CN-K ternary diagram (Fig. 7). The CIA values of 50-65, 65-85, and 85-100 percentage indicate weak, intermediate, and strong weathering intensity, respectively (Price and Velbel, 2003; Hatano et al., 2019; Liu et al., 2020). In the present study, there was an intermediate chemical weathering intensity in P1, P3, P5, and P6, with the CIA values ranging from 65 to 75%, on top of weak to intermediate chemical weathering intensity in P2, P4, and P7 with the CIA values between 55 to 75% (Fig. 7).

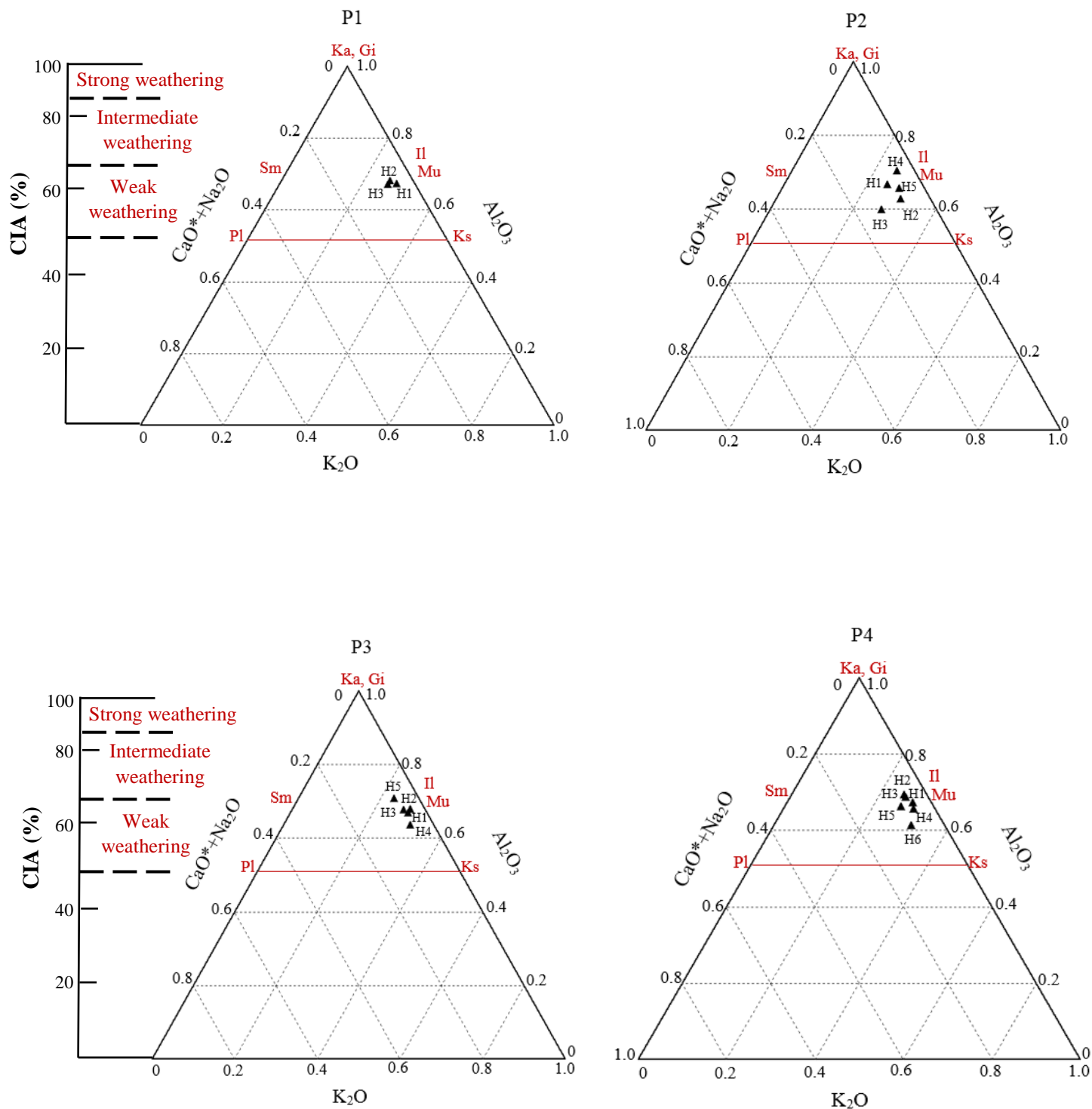
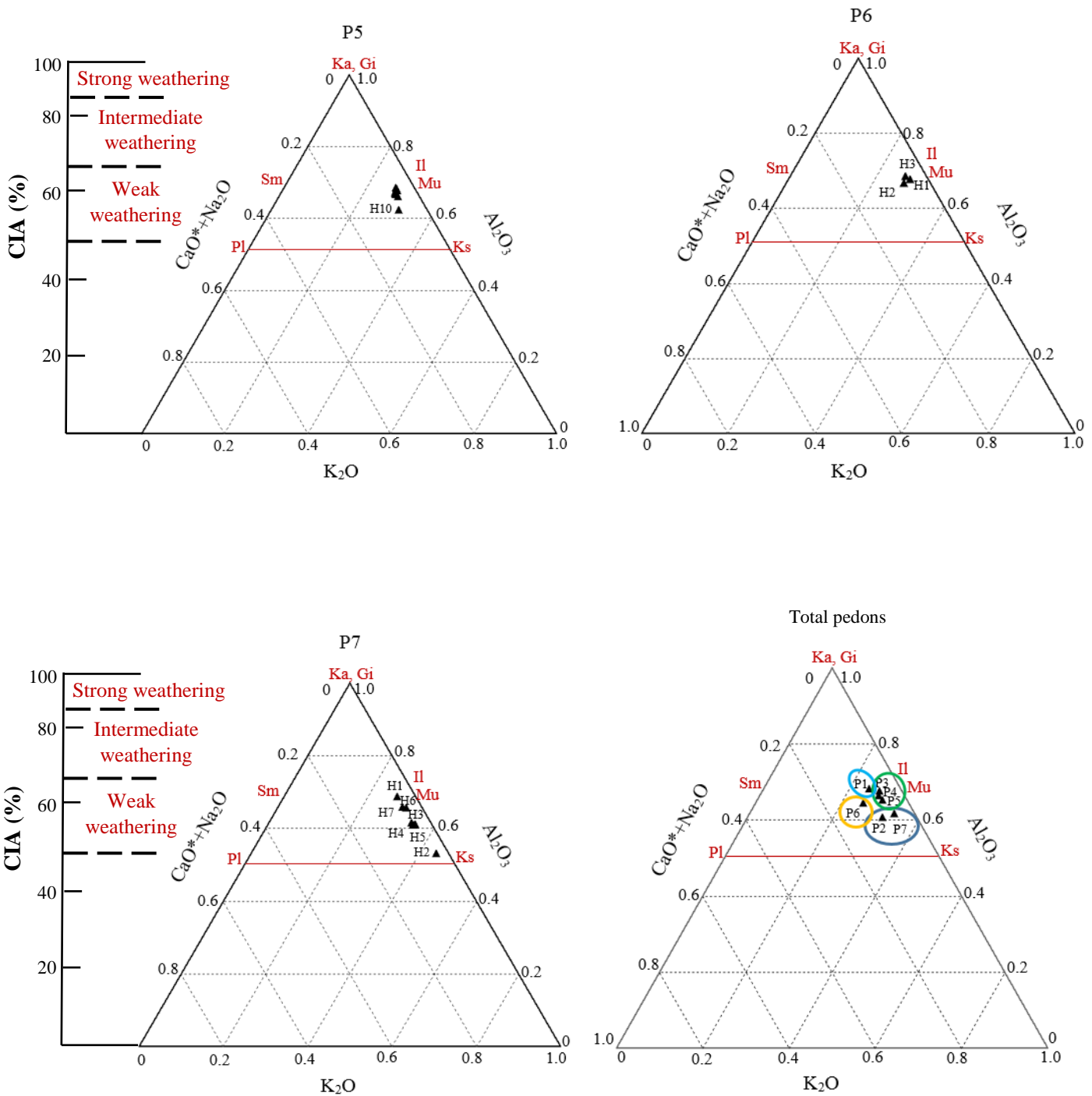


Figure 7. The Al_2O_3 -($CaO + Na_2O$)- K_2O (A-CN-K) ternary diagram for the studied pedons and their horizons. The position of minerals plagioclase (Pl), K-feldspar (Ks), smectite (Sm), illite (il), muscovite (Mu), Ka (kaolin), gibbsite (Gi) is given in the orientation of the ternary diagram.

H_i ($i=1, 2, \dots, n$) shows the number of horizons in each pedon



Continued Figure 7. The Al_2O_3 -($CaO + Na_2O$)- K_2O (A-CN-K) ternary diagram for the studied pedons and their horizons. The position of minerals plagioclase (Pl), K-feldspar (Ks), smectite (Sm), illite (il), muscovite (Mu), Ka (kaolin), gibbsite (Gi) is given in the orientation of the ternary diagram. Hi (i=1, 2, ..., n) shows the number of horizons in each pedon

LDs in this pedon (Table 1), based on the chemical composition, it could be concluded that the aeolian sediments in depths of 0-70 cm (C horizon) and 105-200 cm (3C horizon) are of the same origin. Based on the A-CN-K ternary diagram, it seems that the source of aeolian sediments (C and 3B_{tn} horizons) in the P2 is similar to each other (Fig. 7). In P3, the source of aeolian sediments (C and 3B_y horizons) is the same to each other whereas the source of fluvial sediments (2B_k and 4C₁ horizons) is different in the mentioned horizons. As a result, this issue indicates that the sedimentation process occurred from multiple sources of parent materials (Table 1 and Fig. 7). In other pedons, no specific trend was observed. Due to a confrontation between aeolian and fluvial sediments in the studied area, the conditions were not presumably in favor of the alteration; hence, most variations of chemical composition were possibly derived from changes in the parent material. Previous research has also highlighted that lithology plays a significant role in chemical weathering (Chetelat *et al.*, 2013; Garzanti and Resentini, 2016; Guo *et al.*, 2018).

Grain size and weathering indices

Similar trends were observed for WIP with PI as well as IR with Kr; hence, we only considered two indices. The WIP and Kr indices were plotted with the Al₂O₃/SiO₂ ratio to unravel the effects of the grain size on the weathering indices (Fig. 8). Although the weathering indices changed with the variation of the grain size in all the studied pedons, no common trend was observed for these variations, which could be linked to the simultaneous presence of aeolian and fluvial sediments. The results clearly demonstrated that the type of sediments (aeolian or fluvial sediments) affected the grain size and the weathering indices consequently. Moreover, in P2, there were aeolian sediments, including the particles with high and low Al₂O₃/SiO₂ ratios, possibly reflecting different weathering conditions (Fig. 8). In line with our findings, Wen (1989) reported that the elemental concentrations of dust deposits are partially dependent on grain-size changes. Yang *et al.* (2006) revealed that the grain size influenced the weathering indices in different size fractions within a north–south transect on the Chinese loess plateau.

Although the P6 was formed on the fluvial sediments, there were variations in the weathering indices and Al₂O₃/SiO₂ ratio. These findings confirmed the effect of particle sorting in fluvial sediments on the chemical composition and weathering indices. Hatano *et al.* (2019) showed that the grain size greatly affected the chemical compositions of sediments and sedimentary rocks. Therefore, variation in the weathering indices possibly reflects the variations in the grain size. On the other hand, it could be concluded that the grain size variation of sediments might complicate the evaluation of the degree of chemical weathering; for instance, in some cases, the LDs in soil pedon do not match with the weathering indices.

Conclusion

The current paper characterized the depth distribution of the weathering indices and its relationship with the presence of LDs in seven pedons occurring under different geofoms in Rafsanjan, southeast of Iran. The variability of the Al₂O₃/SiO₂ ratio along a vertical profile closely matched with the depth distribution of the chemical weathering indices and the presence of LDs. According to our results, the Al₂O₃/SiO₂ ratio and the chemical weathering indices could be complementary indicators of the presence of LDs (as a quantitative method). It was also confirmed that most of

the chemical indices are not only related to the type of the sediments, but also to the grain size of the particles in a given sediment and the sorting effect during the sedimentation process. Thus, grain size assessment is necessary for the evaluation and interception of the vertical trend of the weathering indices, especially where there are sediments with variable grain sizes formed on different sedimentary cycles.

Statements and Declarations

The authors declare that they have no known competing financial interests or personal relationships that could have appeared to influence the work reported in this paper.

References

- Ahr SW, Nordt LC, Driese SG. 2012. Assessing lithologic discontinuities and parent material uniformity within the Texas sandy mantle and implications for archaeological burial and preservation potential in upland settings. *Quaternary Research*, 78; 60–71.
- Carpentier M, Chauvel C, Maury RC, Mattiellic N. 2009. The “zircon effect” as recorded by the chemical and Hf isotopic compositions of Lesser Antilliers forearc sediments. *Earth and Planetary Science Letters*, 287; 86–99.
- Chetelat B, Liu CQ, Wang QL, Zhang GP. 2013. Assessing the influence of lithology on weathering indices of the Changjiang River sediments. *Chemical Geology*, 359; 108–115.
- Clift PD, Hodges KV, Heslop D, Hannigan R, Van Long H, Calves G. 2008. Correlation of Himalayan exhumation rates and Asian monsoon intensity. *Nature Geoscience*, 1; 875–880.
- Cremeens DL, Mokma DL. 1986. Argillic horizon expression and classification in the soils of two Michigan hydrosequences. *Soil Science Society of America Journal*, 50; 1002–1007.
- Delvaux B, Herbillon AJ, Vielvoye L. 1989. Characterization of a weathering sequence of soils derived from volcanic ash in Cameroon. Taxonomic, mineralogical and agronomic implications. *Geoderma*, 45; 375–388.
- Derakhshan-Babaei F, Nosrati K, Tikhomirov D, Christl M, Sadough H, Egli M. 2020. Relating the spatial variability of chemical weathering and erosion to geological and topographical zones. *Geomorphology*, 363; 107235.
- Esfandiarpour-Boroujeni I, Mosleh Z, Karimi AR, Martínez-Casasnovas JA. 2020. Detection of lithologic discontinuities in soils: a case study of arid and semi-arid regions of Iran. *Eurasian Soil Science*, 53; 1374- 1388.
- Farpoor MH, Neyestani M, Eghbal MK, Esfandiarpour Boroujeni I. 2012. Soil–geomorphology relationships in Sirjan playa, south central Iran. *Geomorphology*, 138; 223–230.
- Fedo CM, Young GM, Nesbitt HW. 1997. Paleoclimatic control on the composition of the Paleoproterozoic Serpent Formation, Huronian Supergroup, Canada: a greenhouse to icehouse transition. *Precambrian Research*, 86; 201–223.
- Gaillardet J, Dupre B, Alle`gre CJ. 1999. Geochemistry of large river suspended sediments: silicate weathering or recycling tracer? *Geochimica et Cosmochimica Acta*, 63; 4037–4051.
- Garzanti E, Ando S, France-Lanord C, Censi P, Vignola P, Galy V, Lupker M. 2011. Mineralogical and chemical variability of fluvial sediments 2. Suspended-load silt (Ganga–Brahmaputra, Bangladesh). *Earth and Planetary Science Letters*, 302; 107–120.
- Garzanti E, Ando S, France-Lanord C, Vezzoli G, Censi P, Galy V, Najman Y. 2010. Mineralogical and chemical variability of fluvial sediments 1. Bedload sand (Ganga–Brahmaputra, Bangladesh). *Earth and Planetary Science Letters*, 299; 368–381.

- Garzanti E, Padoan M, Setti M, López-Galindo A, Villa IM. 2014. Provenance versus weathering control on the composition of tropical river mud (southern Africa). *Chemical Geology*, 366; 61–74.
- Garzanti E, Resentini A. 2016) Provenance control on chemical indices of weathering (Taiwan river sands). *Sedimentary Geology*, 336; 81-95.
- Gee GW, Bauder JW. 1986. Particle size analysis, in: Klute A. (Ed.), *Methods of Soil Analysis*, Agron. Monger, Madison, pp. 383-411.
- Geological survey and mineral exploration of Iran. 2020. <http://www.gsi.ir>.
- Guo Y, Yang S, Su N, Li C, Yin P, Wang Z. 2018. Revisiting the effects of hydrodynamic sorting and sedimentary recycling on chemical weathering indices. *Geochimica et Cosmochimica Acta*, 227; 48-63.
- Harnois L. 1988. The CIW index: a new chemical index of weathering. *Sedimentary Geology*, 55; 319–322.
- Hatano N, Yoshida K, Sasao E. 2019. Effects of grain size on the chemical weathering index: A case study of Neogene fluvial sediments in southwest Japan. *Sedimentary Geology*, 386; 1–8.
- Honda M, Shimizu H. 1998. Geochemical, mineralogical and sedimentological studies on the Taklimakan Desert sands. *Sedimentology*, 45; 1125-1143.
- IUSS Working Group WRB. 2015. World Reference Base for Soil Resources 2014, update 2015 international soil classification system for naming soils and creating legends for soil maps. In: *World Soil Resources Reports No. 106*. FAO, Rome.
- Lacey JP, Evrard O, Smith HG, Blake WH, Olley JM, Minella JPG, Owens PN. 2017. The challenges and opportunities of addressing particle size effects in sediment source fingerprinting: A review. *Earth-Science Reviews*, 169; 85-103.
- Lanyon LE, Heald WR. 1982. Magnesium, calcium, strontium, and barium, in: Page, A.L. et al. (Eds.), *Methods of soil analysis*. Agron. Monger, Madison, pp. 247–262.
- Liu S, Li J, Zhang H, Cao P, Mi B, Khokiattiwong S, Kornkanitnan N, Shi X. 2020. Complex response of weathering intensity registered in the Andaman Sea sediments to the Indian Summer Monsoon over the last 40 kyr. *Marine Geology*, 426; 106206.
- Lupker M, France-Lanord C, Galy V, Lave JM, Gaillardet J, Gafurel AP, Guilmette C, Rahman M, Singh SK, Sinha R. 2012. Predominant floodplain over mountain weathering of Himalayan sediments (Ganga basin). *Geochim. Cosmochim. Acta*, 84; 410-432
- Moignien R. 1966. Review of Research on Laterites. Natural Resources Research W. United Nations Educational, Scientific and Cultural Organization, Paris. 148 pp.
- Nelson RE. 1982. Carbonate and gypsum, in: Page, A.L. (Ed.), *Methods of Soil Analysis*. Agron. Monger, Madison, pp. 181-196.
- Nelson DW, Sommers LE. 1982. Total Carbon, Organic matter, in: Page, A.L., et al. (Ed.), *Method of Soil Analysis*. Agron. Monger, Madison, pp. 539–577.
- Nelson RE, Klameth LC, Nettleton WD. 1978. Determining soil gypsum content and expressing properties of gypsiferous soils. *Soil Sci Soc Am J*, 42; 659-661.
- Nesbitt HW, Young GM. 1982. Early Proterozoic climates and plate motions inferred from major element chemistry of lutites. *Nature*, 299; 715–717.
- Nesbitt HW, Young GM, McLennan SM, Keays RR. 1996. Effects of chemical weathering and sorting on the petrogenesis of siliciclastic sediments, with implications for provenance studies. *Journal of Geology*, 104; 525-542.
- Okewale IA. 2020. Applicability of chemical indices to characterize weathering degrees in decomposed volcanic rocks. *Catena*, 189; 104475.
- Parker A. 1970. An index of weathering for silicate rocks. *Geological Magazine*, 107; 501–504.
- Price JR, Velbel MA. 2003. Chemical weathering indices applied to weathering profiles developed on heterogeneous felsic metamorphic parent rocks. *Chemical Geology*, 202; 397–416.
- Qin X, Mu Y. 2011. Elimination and evaluation of grain size's effect in analysis of chemical weathering of loess–paleosol sequences. *Chemie der Erde*, 71; 53–58.
- Roser BP. 2000. Whole–rock geochemical studies of clastic sedimentary suites. *Memory of Geological Society of Japan*, 57; 73–89.

- Roy PD, Caballero M, Lozano R, Smykatz-Kloss W. 2008. Geochemistry of Late Quaternary sediments from Tecocomulco lake, central Mexico: implication to chemical weathering and provenance. *Chemie der Erde*, 68; 383–393.
- Ruxton BP. 1968. Measures of the degree of chemical weathering of rocks. *The Journal of Geology*, 76; 518–527.
- Schoeneberger PJ, Wysocki DA, Benham EC, Soil Survey Staff. 2012. Field book for describing and sampling soils. Natural Resources Conservation Service. National Soil Survey Center, Lincoln, NE.
- Soil Science Division Staff. 2017. Soil Survey Manual. U.S. Department of Agriculture, Handbook No. 18. pp. 605
- Soil Taxonomy. 2014. Keys to Soil Taxonomy, 12th ed. USDA-Natural Resources Conservation Service, Washington, DC.
- Song C, Ji H, Beckford HO, Chang C, Wang S. 2019. Assessment of chemical weathering and physical erosion along a hillslope, southwest China. *Catena*, 182; 104133.
- Tsai CC, Chen ZS. 2000. Lithologic discontinuities in Ultisols along a topo-sequence in Taiwan. *Soil Science*, 165; 587–596.
- Vasu D, Karthikeyan K, Atole S, Paul R, Gaikwad SS, Humadevi K, Shabana S, Neha G, Roshani N, Tiwary P, Chandran P. 2020. Elucidating the geogenic and pedogenic pathways of formation of soils of Peninsular India – Signatures of past landscape modifications. *Catena*, 192; 104591.
- Wen QZ. 1989. *The Geochemistry of Chinese Loess*. Science Press, Beijing. [In Chinese]
- Yang SL, Ding F, Ding ZL. 2006. Pleistocene chemical weathering history of Asian arid and semi-arid regions in loess deposits of China and Tajikistan. *Geochimica et Cosmochimica Acta*, 70; 1695–1709.
- Zinck JA. 1989. *Physiography and soils. Lecture-notes for soil students*. Soil Science Division. Soil survey courses subject matter: K6 ITC, Enschede, The Netherlands.